

## Simultaneous Multi-slice Airway Compliance Measurement using Sparse Golden-angle Radial CAIPIRINHA

Ziyue Wu<sup>1</sup>, Michael C.K. Khoo<sup>1</sup>, and Krishna S. Nayak<sup>1</sup>

<sup>1</sup>University of Southern California, Los Angeles, CA, United States

**TARGET AUDIENCE:** Sleep medicine physicians and MR physicists who are interested in upper airway imaging.

**INTRODUCTION:** Obstructive sleep apnea (OSA) is characterized by repetitive upper airway (UA) collapse during sleep. UA compliance, defined as the ratio of UA cross-sectional area and pressure, has been used to measure airway collapsibility<sup>1</sup>. Single-slice compliance measurement has been performed using real-time imaging<sup>2</sup>, however extended spatial coverage is essential in order to characterize collapse pattern. Here we present a method for simultaneous multi-slice compliance measurement based on sparse golden-angle radial CAIPIRINHA<sup>3</sup>, with acceleration factor up to **33.3**.

**METHODS:** *I. Data acquisition:* Experiments were performed on a clinical 3T scanner (EXCITE HDxt, GE) using a 6-channel carotid receive coil. Physiological signals including facemask pressure, abdomen bellow displacement, oxygen saturation and heart rate were simultaneously recorded to determine wakefulness/sleep. The mask was occasionally occluded to generate enough negative pressure for measuring compliance. To image  $N$  slices, a total of  $N$  unique multi-band RF pulses were applied alternatively. The  $n^{\text{th}}$  pulses was designed such that the phase difference between adjacent slices was  $2\pi n/N, n \in [0, N - 1]$ . Continuous radial acquisition with  $1/N$  golden-angle increment was used. Imaging parameters were: radial FLASH,  $5^\circ$  flip angle, 7mm/3mm slice thickness /spacing, 200 samples per readout, FOV 200x200mm<sup>2</sup>, TR 4ms.

*II. Reconstruction:* 24 spokes were used to reconstruct each temporal frame without view-sharing, which led to 96ms temporal resolution. Each slice was reconstructed separately by iteratively minimizing the cost function:  $f_i = ||P_i E S_i m_i - P_i k||_2^2 + \lambda_i ||\phi m_i||_1, i \in [1, N]$ , where  $P_i$  is the RF phase cycling pattern,  $E$  is NUFFT encoding<sup>4</sup>,  $S_i$  is coil sensitivity map,  $k$  is the acquired k-space data,  $\phi$  is temporal variation, and  $m_i$  is the image to be solved.  $\lambda_i$  was chosen empirically.

*III. Post-processing:* The airway was segmented in each frame using a semi-automated region-growing algorithm<sup>2</sup>. The airway area was normalized by the maximum cross-sectional area among all slices during tidal breathing, in order to enable inter-subject comparison. For each slice, all data from one occluded breath were used to perform a linear regression (airway area vs pressure), from which the compliance (line slope) and projected closing pressure ( $P_{\text{crit}}$ ) can be estimated.

**RESULTS & DISCUSSION:** Figs. 1 & 2 contain some representative results from one OSA patient during sleep using 4-slice simultaneous acquisition. **Fig.1** shows two frames, one with the airway partially collapsed (top & middle rows) and the other with it open (bottom row). Gridding reconstruction was not able to recover usable images due to severe aliasing artifacts, interference from other slices, and low SNR. The proposed reconstruction is able to recover all of the relevant UA boundary information. Minor residual streaking artifacts persists but did not affect airway segmentation in our experience. This could be mitigated by sacrificing temporal resolution. However, we purposely chose a high temporal resolution  $\leq 100\text{ms}$  because it is critical to fully resolve the airway dynamics. **Fig.2-a** shows the cross-sectional area of each slice together with the mask pressure. **Fig.2-b** shows the linear regression lines for all four slices. **Table 1** compares the compliance and  $P_{\text{crit}}$  between one OSA patient and one healthy volunteer. The healthy volunteer has more uniform compliance and  $P_{\text{crit}}$  across the airway. While  $P_{\text{crit}}$  and compliance are lower in most of the upper airway for the healthy volunteer, it can be the other way at certain locations.

**CONCLUSION:** We demonstrated simultaneous acquisition of 4 slices with our proposed method, which corresponds to **33.3x** undersampling compared to fully sampled Cartesian acquisition. Our preliminary result suggests that both the compliance and  $P_{\text{crit}}$  can indeed vary among different slices, which confirms the value of multi-slice measurements. To our best knowledge, it also shows for the first time that *a narrower airway site does not always have higher compliance and  $P_{\text{crit}}$ , and therefore is not always easier to collapse* (S2/S4 versus S1). This finding may impact future OSA surgical planning.

**REFERENCES:** [1] Kim et al., ISMRM 2012, p3688 [2] Wu et al., ISMRM 2014, 4323. [3] Yutzy et al., MRM 2011 65(6):1630-37. [4] Fessler et al., JMRI 2007 188(2):191-95.

**GRANT SPONSOR:** NIH R01-HL105210.

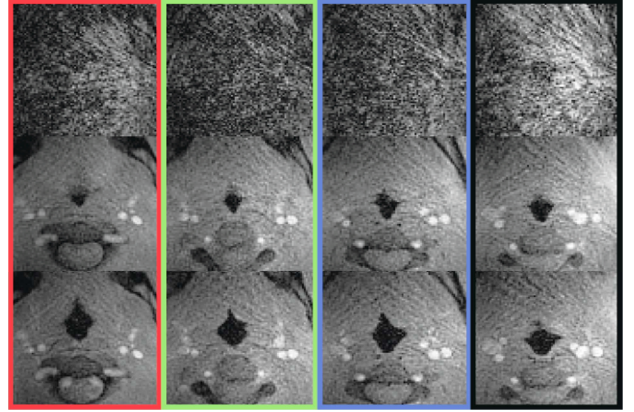


**Fig 1.** Representative frames of airway dynamics from one sleep apnea patient. Four-slice simultaneous acquisition, from left to right: velopharynx to oropharynx. Top: one frame when airway is partial collapsed (with gridding); middle: the same frame after proposed reconstruction; bottom: another frame with airway open.

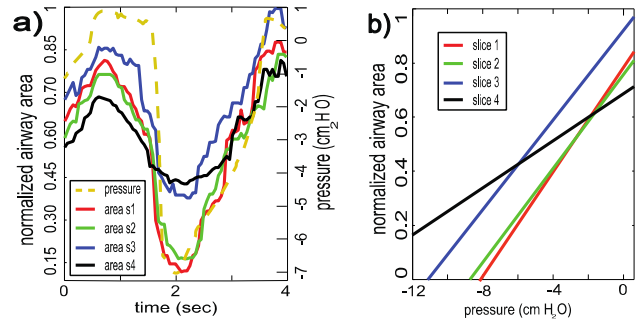


**Fig 2.** a) Plot of airway pressure and segmented airway areas at different locations. S1-S4 correspond to the slice from left to right in Fig. 1. b) Linear regression plots for all 4 slices. The slope is defined as compliance. Also note the projected closing pressure (airway area = 0).

**Table 1.** Comparison of compliance &  $P_{\text{crit}}$  between one OSA patient and one healthy volunteer.

	OSA		healthy	
	Compliance (cmH <sub>2</sub> O <sup>-1</sup> )	$P_{\text{crit}}$ (cmH <sub>2</sub> O)	Compliance (cmH <sub>2</sub> O <sup>-1</sup> )	$P_{\text{crit}}$ (cmH <sub>2</sub> O)
S1	0.094	-8.1	0.049	-12.7
S2	0.082	-8.7	0.062	-12.2
S3	0.085	-11.2	0.057	-11.8
S4	0.041	-16.9	0.051	-13.3